Supplement of Weather Clim. Dynam., 7, 659–679, 2026
https://doi.org/10.5194/wcd-7-659-2026-supplement

Supplement of

Relating extratropical atmospheric heat transport to cyclone life cycle characteristics and numbers in Southern Hemispheric winter

Jan Zibell et al.

Correspondence to: Jan Zibell (jan.zibell@env.ethz.ch)

S1 Abbreviations and terminology

To facilitate the lecture of this study, a list of abbreviations (Table S1) and frequently used mathematical terms (Table S2) is provided.

Table S1: Description of selected physical terms used throughout the thesis sorted by where they are introduced.

Abbreviation	Meaning
DJF	December, January, February
EQ	Equator
HP	High-pass (filtering method, framework)
JJA	June, July, August
(r)lat	(rotated) latitude
(r)lon	(rotated) longitude
MA	Monthly anomaly (framework)
MSE	Moist static energy
NH	Northern Hemisphere
SFA	Standardized flux anomalies
SH	Southern Hemisphere
SLP	Sea level pressure
SP	South Pole
TOA	Top of atmosphere
ZA	Zonal anomaly (framework)

S2 Further details on the MSE flux attribution to cyclones

In our study, we identify events of large eddy MSE fluxes based on a seasonally and latitudinally varying flux threshold. This threshold is computed by aggregating all values of a latitude band of the same time of every year and computing a percentile based on that distribution. This is illustrated in Fig. S1. The identified features are then attributed to surface cyclones using SLP-derived masks as shown in Fig. 2. The transient MSE fluxes differ for each flux decomposition method (Fig. S2a–c) and so do the identified flux features (Fig. S2d–f). As a result, at a single instance a cyclone may be attributed some equatorward flux of positive MSE (dark blue patches at 60° E in Fig. S2g,h) or not (Fig. S2i). Note that not all flux features overlap with cyclone masks (yellow patches in Fig. S2g–i).

S3 Sensitivity and variability of near-cyclone eddy MSE fluxes

To further strengthen the conclusions drawn from the cyclone composites, a significance test is performed for the monthly anomaly framework. For this we address the standardized flux anomalies (SFA) from the climatological seasonal mean, $v'm'^{\mathrm{clim}}_{\mathrm{MA}}$, defined as

$$\mathrm{SFA}(lon, lat, time, pressure) = \frac{v'm'_{\mathrm{MA}}(lon, lat, time, pressure) - v'm'^{\mathrm{clim}}_{\mathrm{MA}}(lon, lat, pressure)}{\sigma(v'm'_{\mathrm{MA}})(lon, lat, pressure)} \tag{S1}$$

Table S2: Description of selected physical terms used throughout the thesis sorted by where they are introduced.

Term	Description
$v'm'_{\mathrm{MA}}$	Meridional transient MSE fluxes derived from monthly anomalies
$v'Lq'_{\mathrm{MA}}$	Meridional transient moisture fluxes derived from monthly anomalies
$v'm'_{\mathrm{HP}}$	Meridional transient MSE fluxes derived from high-pass filtering
$v^*m^*_{\mathrm{ZA}}$	Meridional transient MSE fluxes derived from instantaneous anomalies from the zonal mean
$[v'm'_{\mathrm{MA}}]$	Zonal mean (or zonally integrated) transient MSE fluxes
$\overline{v'm'}^{\,\mathrm{MA}}$	Monthly or seasonal mean transient MSE fluxes
$\langle v'm'_{\mathrm{MA}}\rangle$	Vertically integrated transient MSE fluxes
$\langle [v'm'_{\mathrm{MA}}]\rangle$	Vertically integrated zonal mean (or zonally integrated) transient MSE fluxes
$\langle [\overline{v'm'}^{\,\mathrm{MA}}]\rangle$	Seasonal mean zonally and vertically integrated ('overall') transient MSE fluxes
$\langle v'm'^{\,\mathrm{cycl}}_{\mathrm{MA}}\rangle$	Vertically integrated transient MSE fluxes attributed to cyclones
$\langle [v'm'^{\,\mathrm{cycl}}_{\mathrm{MA}}]\rangle$	Zonal integral of vertically integrated transient MSE fluxes attributed to cyclones
$\langle [\overline{v'm'}^{\,\mathrm{cycl}}_{\mathrm{MA}}]\rangle$	Seasonal mean zonal integral of vertically integrated transient MSE fluxes attributed to cyclones
$\langle [\overline{vm}]\rangle$	Seasonal mean ('total') heat transport
$v'm'^{\,\mathrm{clim}}_{\mathrm{MA}}$	Climatology of meridional transient MSE fluxes
$\langle [\overline{v'^{,*}m'^{,*}}^{\,\_\_}]\rangle$	Seasonal mean zonal and vertical integral of 'overall' transient, cyclone-attributed MSE fluxes for a given framework
$\langle [\overline{v'^{,*}m'^{,*}}^{\,\mathrm{cycl}}_{\_\_}]\rangle$	Seasonal mean zonal integral of vertically integrated, cyclone-attributed transient MSE fluxes for a given framework
n_{all}	Seasonal number of cyclones that were attributed non-zero transient MSE flux at a latitude band of interest

with σ the standard deviation over the climatological period. Locations in the composite where mean(SFA) = 0, we regard the $v'm'_{\mathrm{MA}}$ of the individual events that we used for compositing as not significantly different from climatological $v'm'_{\mathrm{MA}}$ fluxes. In other words, the null hypothesis, mean(SFA) = 0, is rejected if within the composite, fluxes are sampled that are on average different from climatology. We perform a two-sided, one sample t-test at each composite grid-cell (Fig. S3). Overall, the dynamical features that were identified in the composites are based on flux anomalies that on average are significantly different from zero. Note that low $v'm'_{\mathrm{MA}}$ can be significant in the composite as it is lower than climatology.

Compared to the monthly anomaly (MA) framework, it is also the intensification phase (and not the mature stage) during which fluxes are largest when adopting the high-pass (HP) and zonal anomaly (ZA) decompositions (not shown). A comparison of the fluxes at peak cyclone intensification reveals that at 850 hPa, high-pass filtered fluxes are marginally lower than MA fluxes (Fig. S4a,b). Moreover, the contrast between warm and cold sectors is reduced in the ZA framework (Fig. S4c), which could be explained by strong warm sector anomalies raising the instantaneous zonal mean MSE such that cold sector anomalies become larger compared to the other methods. Note that for the NH, the differences between MA and ZA are more pronounced (not shown) due to the time-stationary signal being declared as SE flux (Eq. 2). These descriptions are also valid for vertically integrated fluxes (Fig. S4d–f).

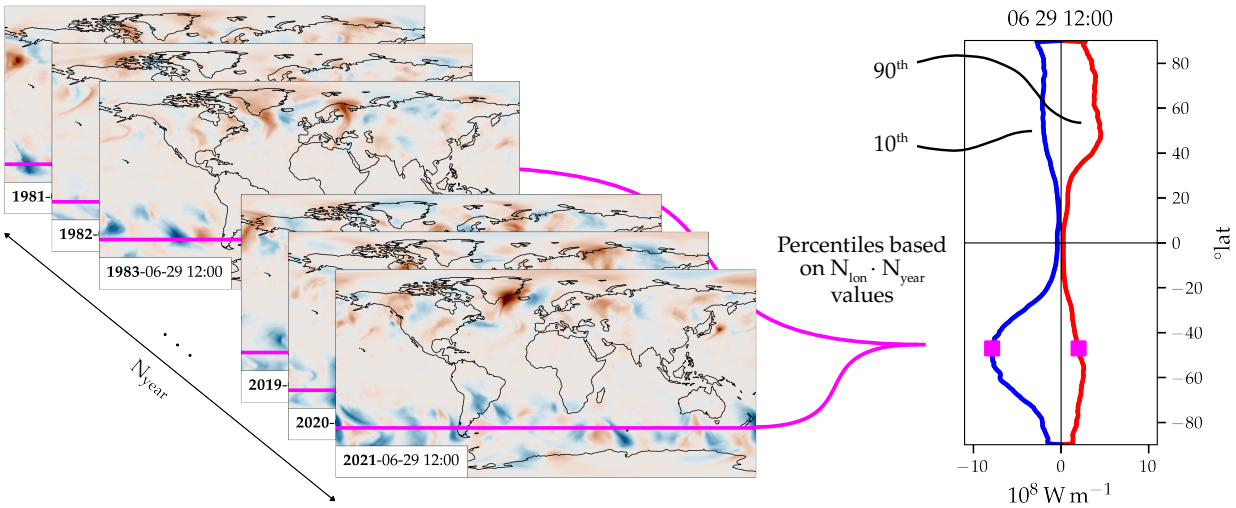

Figure S1: Illustration of the determination of the percentile threshold for eddy MSE flux events based on the monthly anomaly framework: For every six-hourly time step of a year — 29 June, 12:00 UTC, for instance — eddy MSE flux thresholds for poleward and equatorward fluxes are calculated at each latitude. These are based on the values of that latitude band and every corresponding time of year during the analysis period. Thus, the sample size which the percentile is computed from is the number of years (N_{lon}) times the number of grid-cells at a latitude circle (N_{lon}). The 10^{th} and 90^{th} percentiles of the vertically integrated eddy MSE fluxes (color shading on the left panel) for 29 June, 12:00 UTC are shown on the right in blue and red, respectively. The latitude of 47° S is highlighted in magenta.

S4 Method dependence of zonally integrated cyclone-attributed MSE flux

The method sensitivity of the seasonal contributions to transient eddy MSE flux by cyclones, which was discussed in Sect. 4, is shown in Fig. S5. Choosing lower percentiles moves the peak of the attributed fluxes towards the equator because larger masks (warm sectors extending further equatorward than the cyclone mask) are more often attached (Fig. S5a,d,g,j). Higher percentiles reduce the absolute fractions, yet percentages at 50° S remain close to 20 % for $p = 0.95$ (yellow lines in Fig. S5b,e,h,k). The cause of the relatively reduced correlation around 60° S for the ZA framework (Fig. S5i) is not clear but might be related to the presence of planetary waves. A repetition with an upper integral bound of 500 hPa (Fig. S5l) suggests this signal arises from lower levels (and not stratospheric dynamics).

The averages depicted in Fig. 8 conceal the variability of the MSE fluxes attributed to individual cyclones. These are shown in Fig. S6 for the MA framework, in particular each of the 200 cyclones that intensify least and most rapidly across the SH. While the means (solid lines) amount to around 20 PW, individual cyclones can be attributed more than 150 PW across a latitude band of more than 10° (Fig. S6a).

Regarding the method dependency of the zonally integrated MSE fluxes attributed to cyclones of different life cycle characteristics, the corresponding ratios of Fig. 8b,d are shown for lifetime-accumulated and lifetime-averaged fluxes in Fig. S7.

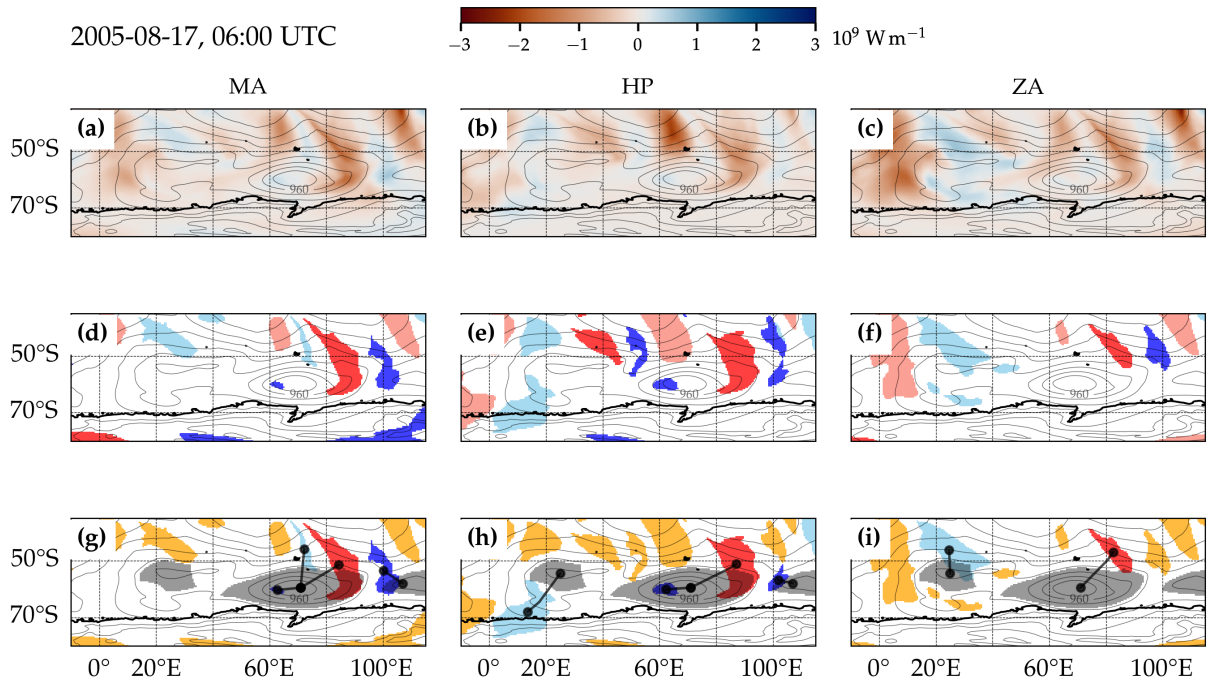

Figure S2: Snapshot of vertically integrated eddy MSE fluxes and their attribution to surface cyclones. **(a)** Vertically integrated eddy MSE fluxes calculated using the monthly anomaly framework (shading in $\mathrm{W\,m^{-1}}$) and SLP (black contours in steps of 10 hPa). **(b)** and **(c)** as in **(a)** but for the HP and ZA frameworks, respectively. **(d)**–**(f)** The binary masks corresponding to the identified flux features are shaded in reddish and bluish colors if MSE fluxes are poleward or equatorward, respectively, and in dark and light tones if fluxes correspond to positive and negative MSE anomalies, respectively. **(g)**–**(i)** In addition to above, surface cyclone masks are shown with grey patches. If flux features are not overlapping with cyclones, the features are colored yellow. Otherwise, black straight lines and dots indicate to which cyclones each feature is attributed to. Coastlines are depicted with black lines.

S5 Sensitivity of the number–flux relationship to choice of flux decomposition method

While the relationships between different seasonal MA MSE fluxes and cyclone numbers are shown by scatterplots (Fig. 10), for conciseness we only show the correlation values for the different flux decompositions and attribution percentiles. In addition to the relationships discussed in Fig. 10, we show correlations with the number of cyclones in the entire SH and with total heat transport ($\langle[\overline{vm}]\rangle$) for 50° S in the left column of Fig. S8 and different latitudes in Fig. S9. Note that measuring intensification rate in Bergeron and intensity based on SLP anomalies from a climatology instead does not yield a qualitatively different picture (not shown).

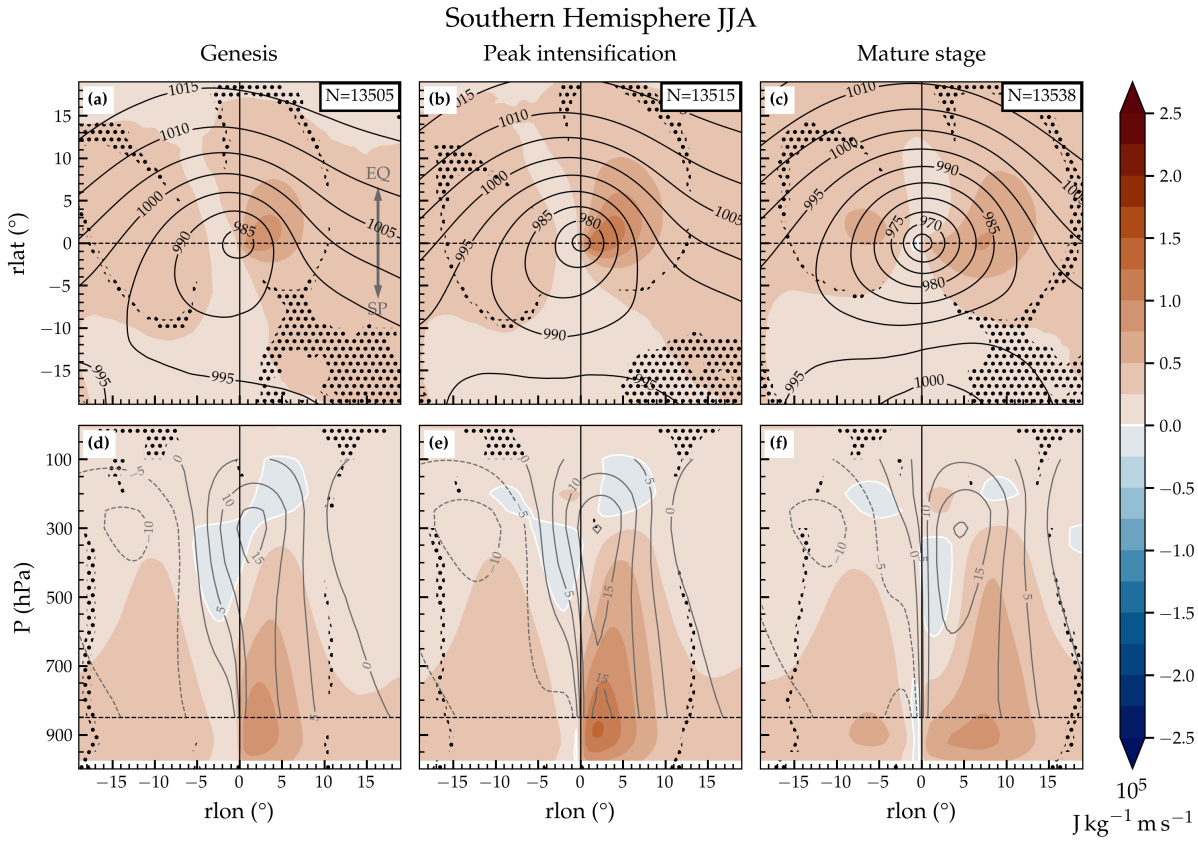

Figure S3: Statistical significance of composited transient MSE flux anomalies as in Fig. 4.Dotted areas indicate where the null hypothesis mean(SFA) = 0 (see Eq. S1) is not rejected at the 95 % confidence level. In **(d)**–**(f)**, grey contours indicate the (vertically sub-sampled) full meridional wind, v, as opposed to v' in Fig. 4d–f.

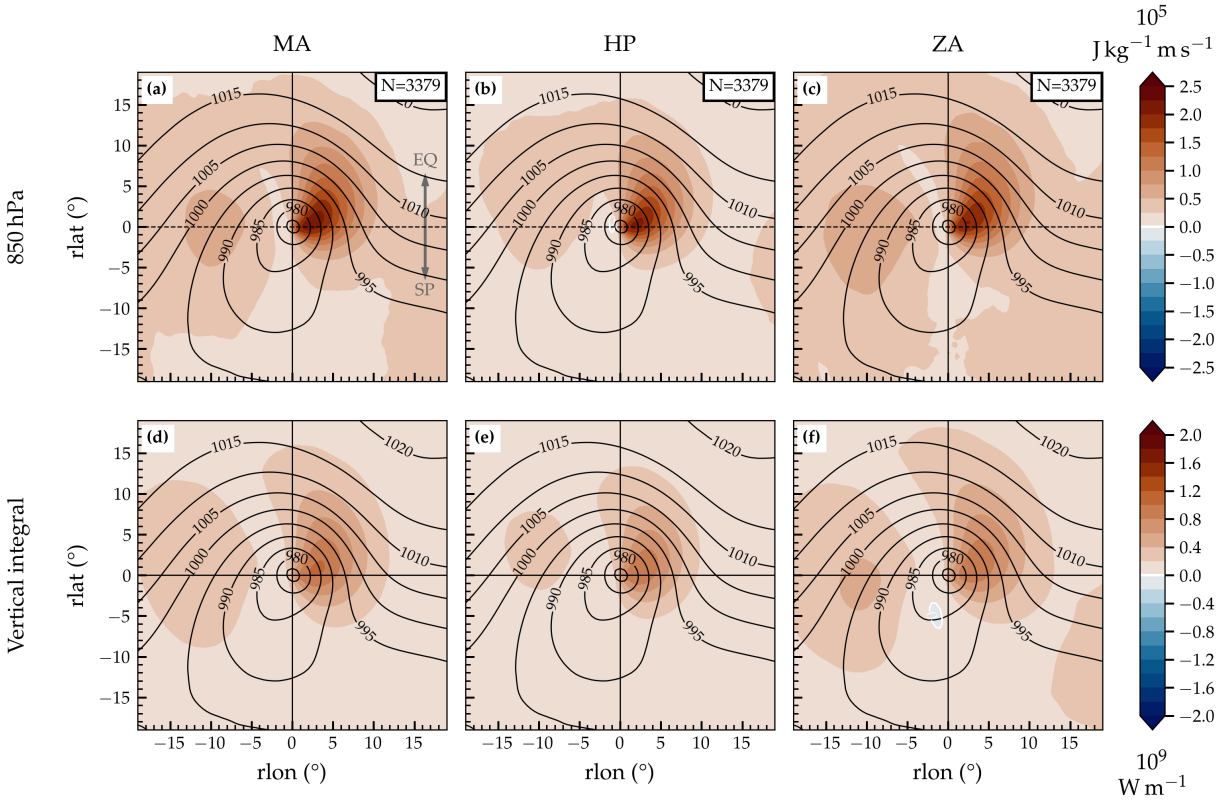

Figure S4: **(a)**–**(c)** Cyclone-centered eddy MSE flux at 850 hPa during time of maximum intensification for the 25 % most strongly intensifying SH cyclones during JJA for three different definitions of eddy flux (see method abbreviations in Sect. 2.3) in J m^{-1} kg s^{-1}. **(d)**–**(f)** Vertically integrated fluxes analogously to **(a)**–**(c)** but in units of W m^{-1}. Black contours indicate composite mean SLP in hPa. The number of cyclones in the composites are included in the upper right in panels **(a)**–**(c)**. A grey arrow is included for better orientation indicating directions of equator (EQ) and South Pole (SP).

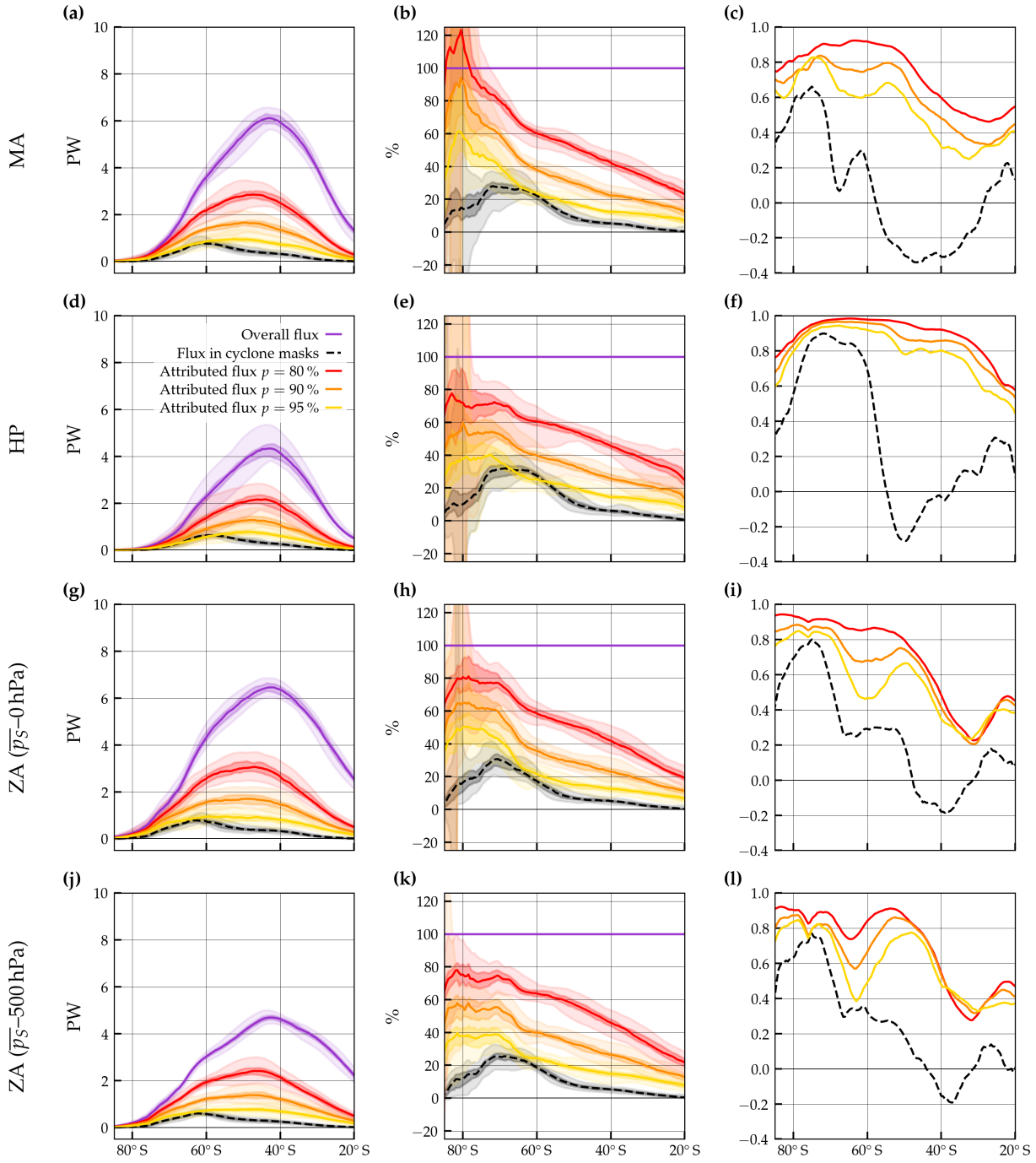

Figure S5: Same as Fig. 7 but repeated for different flux decomposition methods (see Sect. 2.4) and different percentile thresholds for attributing flux to cyclones (yellow, orange, and red distributions and lines corresponding to percentile ranks of 0.8, 0.9, and 0.95.

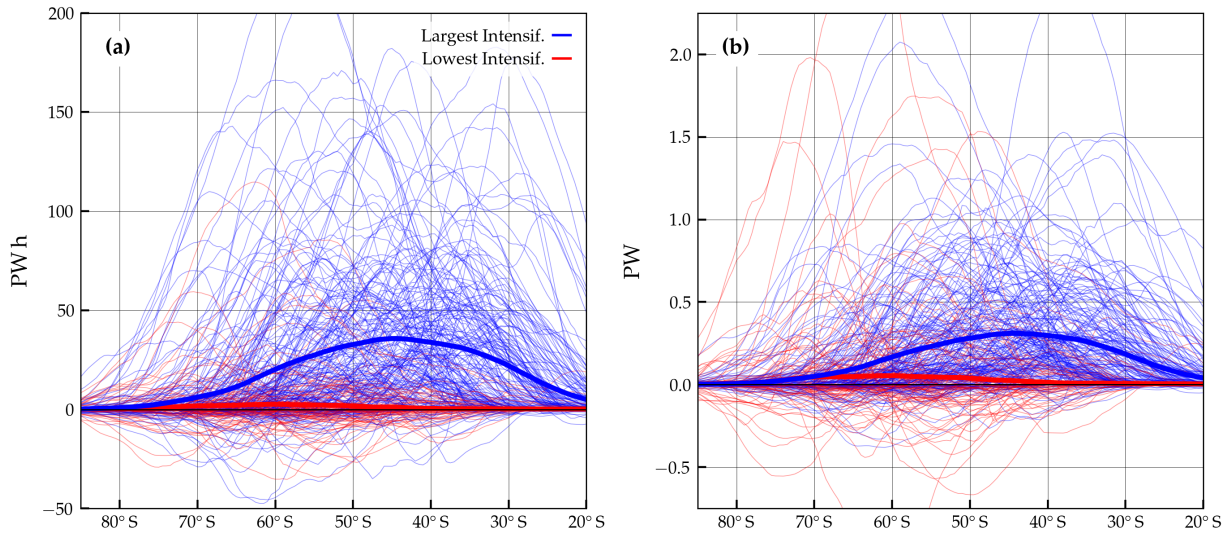

Figure S6: Zonally integrated transient MSE flux attributed to individual extratropical cyclones. **(a)** The lifetime-integrated flux (PW h) of the 200 most strongly intensifying cyclones (blue thin lines) is compared to the flux of the 200 cyclones that intensify least rapidly (red). Thick lines denote the arithmetic means shown in Fig. 8a. **(b)** As in **(a)** but for the lifetime-averaged flux in PW. The flux attribution percentile rank corresponds to $p = 0.9$.

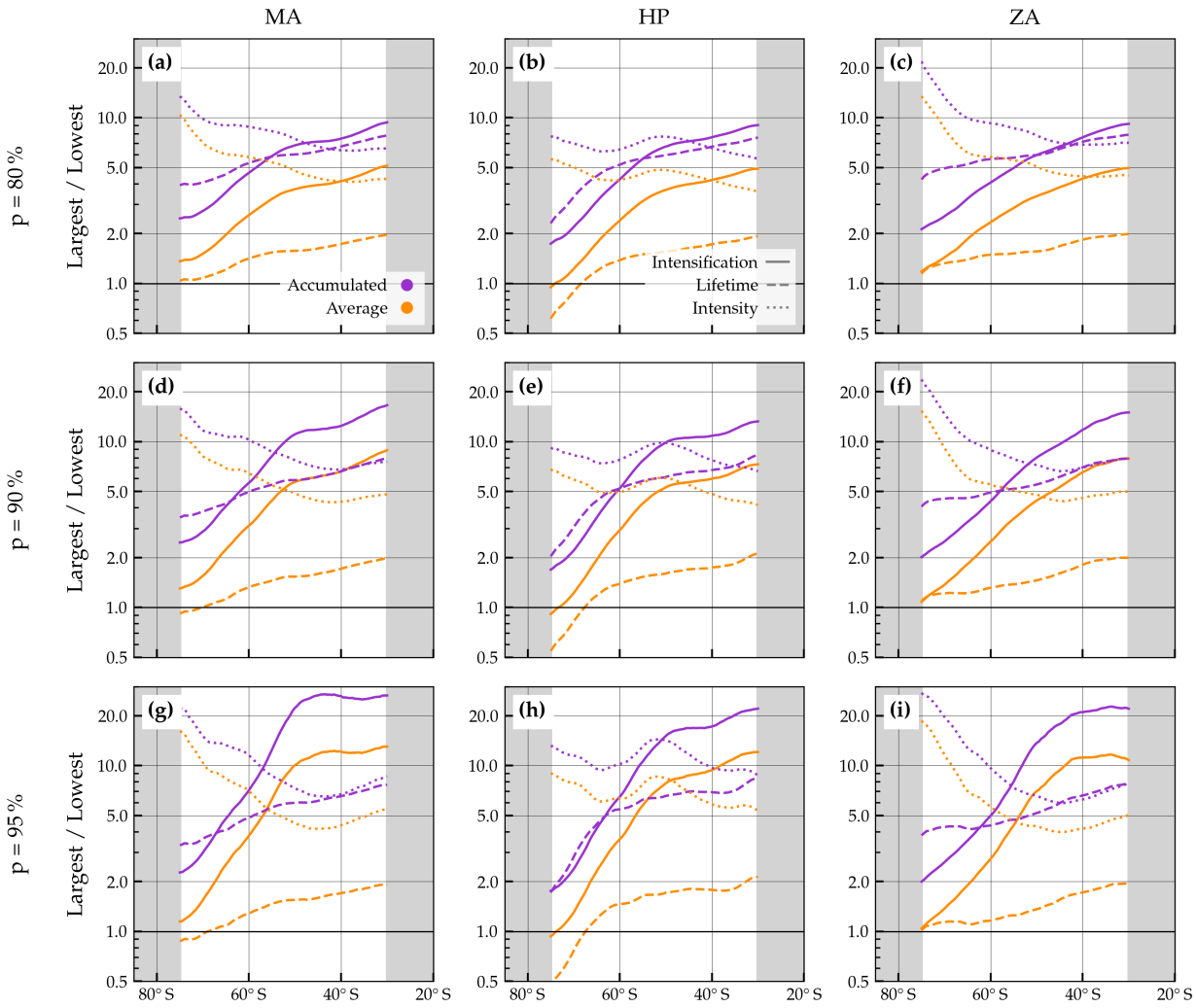

Figure S7: Ratio of the flux related to the 200 cyclones of largest vs. lowest characteristic based on all SH cyclones: Fig. 8b,d are combined and repeated for different flux decomposition methods (columns, see Sect. 2.4) and different percentile thresholds for attributing flux to cyclones (0.8, 0.9, and 0.95, see Sect. 2.4). Purple lines correspond to lifetime-accumulated fluxes, yellow lines to lifetime-averaged fluxes, and the linestyle signifies the cyclone life cycle characteristic.

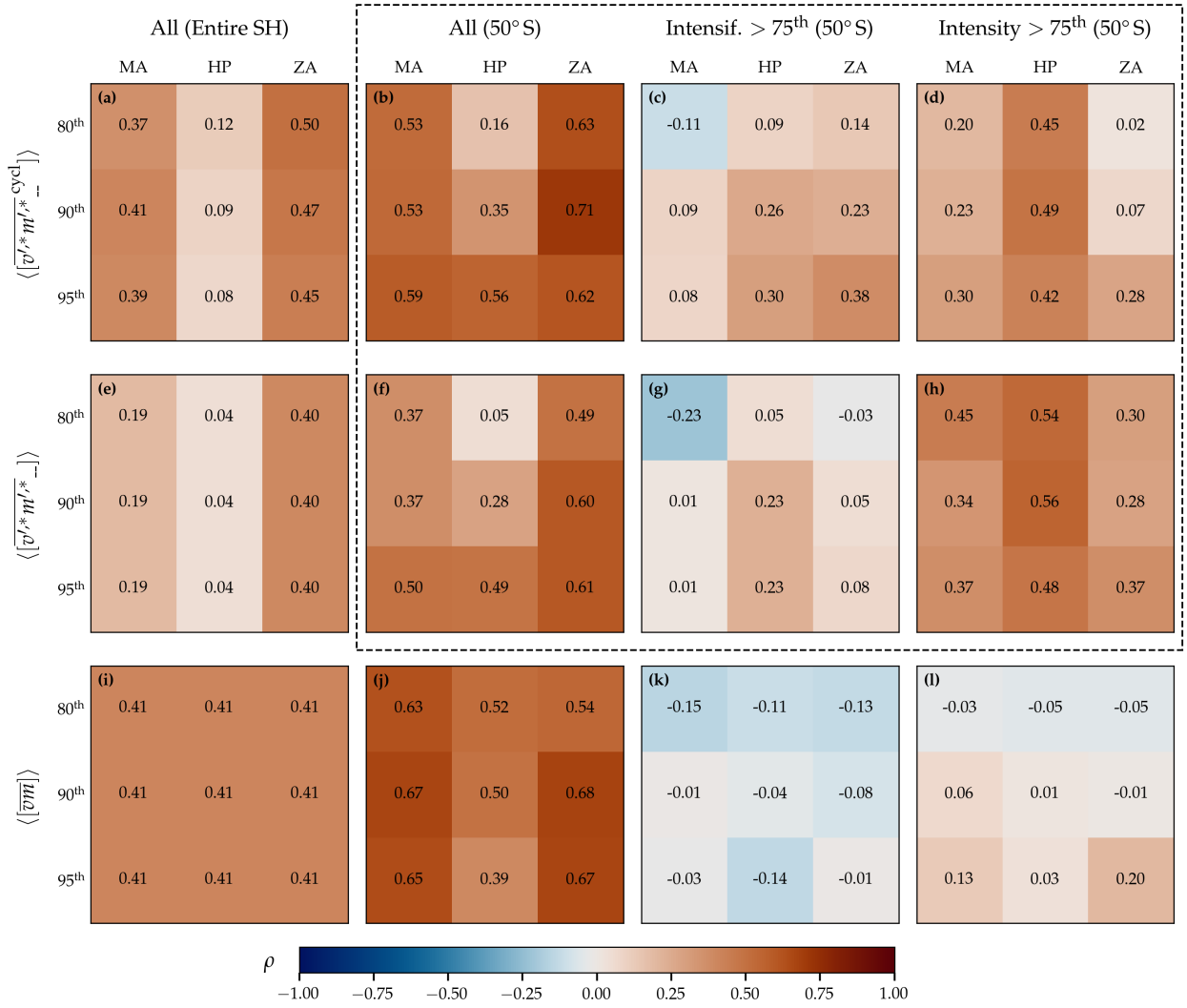

Figure S8: Sensitivity of the correlation (ρ) between seasonally averaged MSE fluxes and seasonal cyclone number to flux decomposition method and flux attribution percentile for different MSE fluxes and groups of cyclones. **(a)** The correlation of the number of all SH cyclones with cyclone-attributed eddy MSE flux, $\langle[\overline{v'^{,*}m'^{,*}}^{\,\mathrm{cycl}}_{--}]\rangle$, at 50° S is shown for each percentile and flux decomposition method. Depending on the decomposition method, these fluxes correspond to temporal anomalies ($'$ for MA and HP) or zonal anomalies (* for ZA). Numerical values are accentuated with colors. Data correspond to SH JJA. This is repeated for **(b)** all cyclones with $\langle[\overline{v'^{,*}m'^{,*}}^{\,\mathrm{cycl}}_{--}]\rangle \neq 0$ at 50° S, **(c)** the cyclones with $\langle[\overline{v'^{,*}m'^{,*}}^{\,\mathrm{cycl}}_{--}]\rangle \neq 0$ at 50° S that have an intensification rate above the 75$^{\mathrm{th}}$ climatological percentile, and **(d)** as **(c)** but for intensity instead of intensification rate. **(e–h)** as **(a–d)** but for the overall eddy MSE flux $\langle[\overline{v'^{,*}m'^{,*}}_{--}]\rangle$. **(i–l)** as **(a–d)** but for the total atmospheric MSE transport $\langle[\overline{vm}]\rangle$. The arrangement of the panels outlined by the black dashed line corresponds to the arrangement of the panels in Fig. 10.

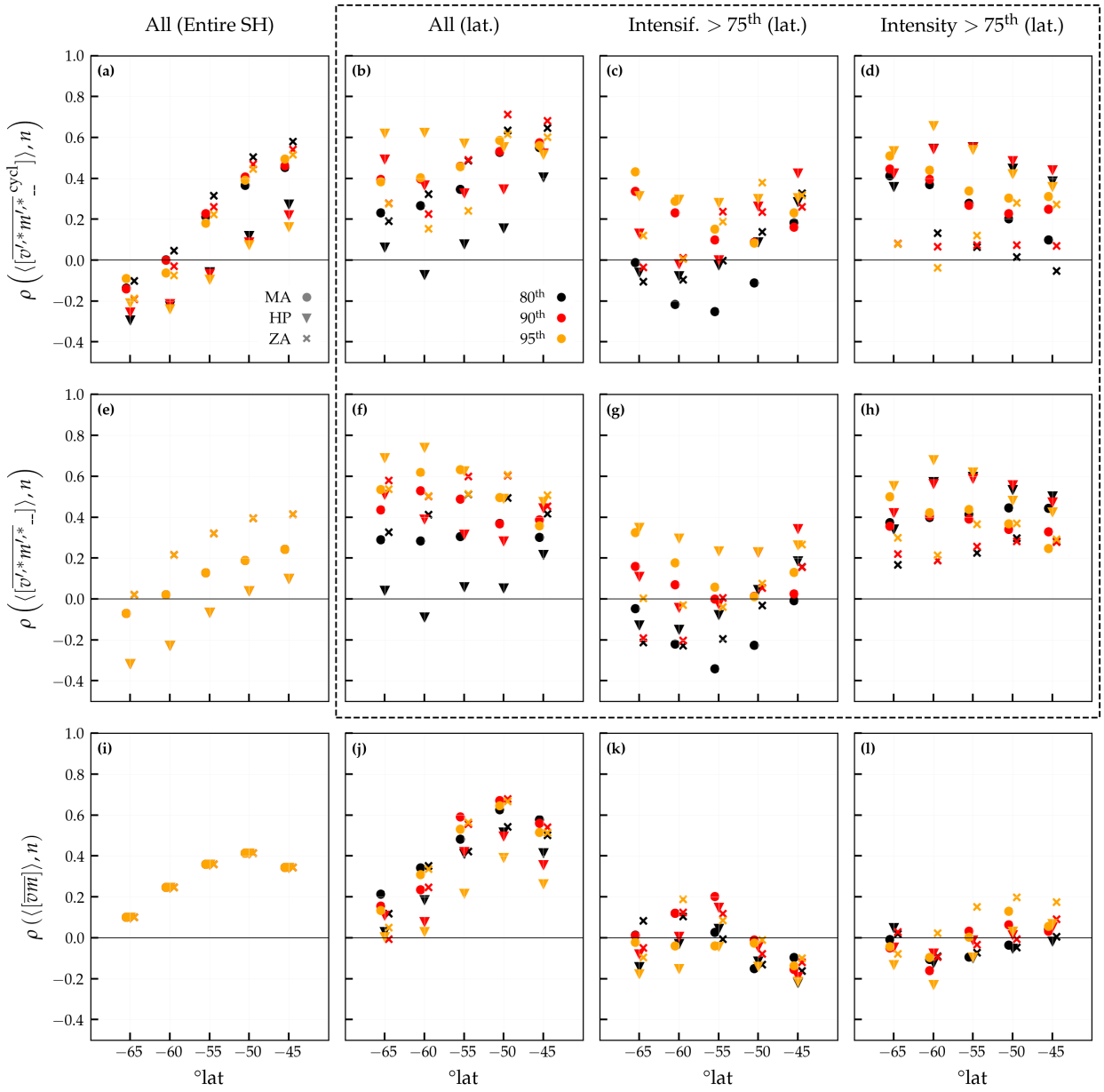

Figure S9: Sensitivity of the correlation (ρ) between seasonally averaged MSE fluxes and seasonal cyclone number to flux decomposition method and flux attribution percentile as in Fig. S8 for different latitudes. **(a)** As in Fig. S8a, the correlation of the number of all SH cyclones with cyclone-attributed eddy MSE flux, $\langle[\overline{v'^{,*}m'^{,*}}^{\,\mathrm{cycl}}_{--}]\rangle$, is shown here in steps of 5° latitude. Colors of the markers indicate the percentile and shapes the decomposition method. Markers for the different flux decomposition methods are slightly offset on the x-axis for better clarity. **(b–l)** as in **(a)** but for the different fluxes and groups of cyclones, arranged as in Fig. S8. The arrangement of the panels outlined by the black dashed line is consistent with Fig. 10.